2013 IEEE/RSJ International Conference on
Intelligent Robots and Systems (IROS)
November 3-7, 2013. Tokyo, Japan

# Haptic Rendering of Interacting Dynamic Deformable Objects Simulated in Real-Time at Different Frequencies

Francois Dervaux[1], Igor Peterlik[2], Jérémie Dequidt[1], Stéphane Cotin[1], Christian Duriez[1]

*Abstract*— **The dynamic response of deformable bodies varies significantly in dependence on mechanical properties of the objects: while the dynamics of a stiff and light object (e. g. wire or needle) involves high-frequency phenomena such as vibrations, much lower frequencies are sufficient for capturing the dynamic response of an object composed of a soft tissue. Yet, when simulating mechanical interactions between *soft* and *stiff* deformable models, a single time-step in the time integration is usually employed to compute the dynamics of both objects. However, this can be a serious issue when the haptic rendering of complex scenes composed of various bodies is considered.**

**In this paper, we present a novel method allowing for the haptic simulation of a scene composed of colliding objects modeled at different frequencies: typically, the dynamics of soft objects is calculated at a frequency of about 50 Hz, while the dynamics of stiff object is simulated at 1 kHz, being directly connected to the computation of the haptic force feedback. The collision response is performed at both low and high frequencies employing data structures which describe the actual constraints and are shared between the high and low frequency loops. We show that during the simulation we show that the objects behave according to two mechanical principles: non-inter-penetration and action-reaction principles. Examples showing the scenes involving different bodies in interaction are given, demonstrating the benefits of the proposed method.**

## I. Introduction

Real-time simulation of deformable bodies is an intensive area of research in the fields of computer graphics, virtual reality and haptics. Among applications targeted by the research, there is a strong need for surgical training systems based on high-fidelity haptic interaction with simulated deformable objects. A significant progress has taken place recently, being related to the *finite element method* (FEM) that allows for accurate modeling of mechanical behavior observed in physical objects. If interaction devices equipped with force feedback are to be considered, the fidelity of the feedback is significantly influenced by the accuracy of the deformation model, but also by the performance of algorithms employed to model the interactions (such as contacts, grasping and others).

In the area of haptic rendering, the main challenge remains the computation of these deformations and interactions in real-time. Although the finite element method is an elegant tool for modeling the dynamic behavior of objects, it remains computationally expensive for complex objects with irregular geometries like the ones that appear in medical simulations. Several strategies have been adopted to accelerate the computations, either by simplifying the simulation of the object behavior, or the interaction taking place among the modeled objects.

The dynamic response may vary significantly depending on the geometric and material characteristics of the object: for example let us suppose a simulation scenario where the scene is composed of two objects: a flexible needle interacting with a deformable organ such as liver. Clearly, as the needle is *stiff* and light, the realistic simulation of its dynamic response requires high frequencies to be taken into account, whereas in the case of the soft tissue which is bulky and *soft* much lower frequencies are sufficient to capture its response correctly. However, the temporal integration used in this scenario usually relies on single time-step in simulation of both objects, mainly if an interaction between the two bodies is modeled in the simulation. Such an approach can be acceptable in situations where the simulation is not required to be run in a real-time: in this case a small simulation time-step is chosen to account for the high frequencies in the needle response. Thereby, it is assumed that the simulation runs much more slowly than the real clock time, as in each small time-step, the costly dynamics of the bulky soft objects has to be recomputed.

Such a solution is not sustainable as soon as the simulation is to be run in real-time. In this context, we focus on a *multi-rate* approach where dynamics of each object in the scene is integrated in real-time with its own time-step. We believe that this approach is especially suited for simulations with haptic rendering. In this case, the dynamics of the stiff object (e.g. the flexible needle) which does not require heavy computations can be simulated in the haptic loop running usually at 1000 Hz, while the dynamics of the soft highly-deformable body (e.g. the liver) is simulated on a much lower frequency (typically synchronized with the visual thread running at about 30 or 60 Hz), since it requires more computationally expensive calculations. This approach is already studied for example in [1] where the objects are simulated at different frequencies, however, at the cost of simplification in the interaction model.

The work presented in this paper is based on [2] where a method allowing for multi-rate interactive simulation of objects simulated at two different frequencies has been proposed. However, the method was suitable only for a quasi-static scenario because it required that *compliance matrices* needed to simulate the interactions between the objects do not depend on time-step. The contribution of this paper is to overcome this limitation and extend the multi-rate approach

This work was supported by French Research Agency (ANR) with the project IDeaS (JCJC SIMI 3).

[1]Shacra Team-Project, INRIA Lille - Nord-Europe and University Lille 1 - LIFL CNRS UMR 8022, France

[2] IHU Strasbourg, 67000 Strasbourg, France

to constraint-based interactions in dynamic scenarios. To our best knowledge, this is the first approach that allows for real-time dynamic simulation of colliding deformable objects, dynamics of which is computed at different frequencies.

The remainder of this paper is organized as follows: a brief overview of the related works is given in section 2. Then the multi-rate dynamics approach is presented in section 3 mainly from the mathematical point of view. In section 4, the computational model is presented and finally the results are presented and discussed in section 5.

## II. Previous Works

Haptic rendering is a productive and very active research field and the literature on the topic is quite vast. We narrow the scope of this section to research works focusing on stable realistic haptic rendering of contacts between soft deformable bodies and the works dealing with asynchronous and/or multi-rate methods.

Haptic interaction with deformable bodies is based on two competing but coupled scientific problems: first, realistic soft body simulation which is computationally intensive and requires large integration time-steps in order to be interactive, and second, realistic haptic rendering which implies fast computations of forces and therefore requires small integration time-steps. In order to achieve an efficient trade-off, works in this field usually rely on two main simplification strategies to achieve the realistic haptic rendering: either the mechanical coupling between the simulation scene and the haptic device is simplified or the complexity of the mechanical models is reduced substantially.

Pioneering works in the field employed the first approach by allowing for local interactions only. For instance Bro-Nielsen and Cotin [3] use bilateral constraints solved with Lagrange Multipliers in order to prevent inter-penetrations whereas Popescu and Compton [4] introduce *small area paradigm* which defines equality constraints that will impact the position of a reduced set of surface vertices of the deformable surface. Unilateral contact combined with computation of *capacitance matrix* is introduced by James and Pai [5] using pre-computed Green's functions that is valid for linear deformations. These methods are limited to single contact point interactions.

Handling complex and multiple friction contacts is introduced by Duriez *et al.* [6] but the method also requires the pre-computation of a *compliance matrix* and the method is also limited to linear deformations. Extension to non-linear deformations is proposed by Barbič and James [7] that allows for multiple contacts and self-collisions of soft bodies with penalty forces. As penalties can not reproduce precise contact and friction conditions, Saupin *et.al* [8] propose to use an approximations of the *compliance* that allows to handle multiple friction contact points using constraints on non-linear models. Similarly, Garre and Otaduy [9] only consider the block-diagonal matrix of the compliance matrix assuming small displacements between time-steps. These later works enable more advanced haptic interactions but are based on assumptions that are not compatible with realistic modeling of dynamic response in stiff and light deformable objects.

Recent works propose computationally fast deformable models in order to achieve high-frequency simulation. For instance, approach proposed by Barbič and James [7] is compatible with reduced deformation models. Similar approach is used in the work of Jacobs *et. al.* [10] where a fast linearized deformable model is computed.

Multi-rate or asynchronous simulation has also been much investigated in the past few years in order to handle computationally expensive deformable models. Harmon *et. al.* [11] describe a multi-rate simulation framework that prevents inter-penetrations, obeys causality and guarantees the conservation of momentum and energy. Their work relies, among other contributions, on asynchronous variational integrators and kinematic data structures. While proven to complete in finite time, such framework is not intended for haptic interactions where small and strictly bounded computation time-step is required. More recent works have addressed the performance issue of multi-rate simulation. Efficient culling of collisions [12] or intermediate representations called *phantom meshes* [13] have been investigated to reduce the computation burden. Nevertheless, the proposed methods are still far from providing a stable haptic rendering of complex objects. Others works deal with haptic interactions provided by dynamic simulation, but are still limited to rigid [14] objects or textiles [15].

The main objective of our approach is to provide realistic haptic rendering of deformable models that can handle a large scope of soft bodies (from stiff and light objects to soft and heavy ones). Our approach combines a multi-rate simulation and an accurate mechanical coupling. The major improvement over the previous work in [2] lies in the capability of our framework to handle full second-order dynamics and is no more restricted to quasi-static scenario.

## III. Dynamic and Asynchronous Deformable Models in Contact

This section presents an overview of our asynchronous framework and details the mathematical notation that is used throughout the paper. More particularly, we detail the models and the numerical methods involved in the simulation of dynamic deformable solids simulated at different frequencies. Additionally, we present the constraint-based solving process associated to the mechanical interactions between these deformable objects.

Our framework relies on simulation loops running at different frequencies. To simplify the explanations and without limiting the generality of the approach, we consider that we have two simulation loops for simulating the interactions between two deformable solids. The first loop, named *low rate* loop, is dedicated to the computation of the dynamics of the object that can be simulated with a large integration time-step (e.g. 20 ms). The solid with such a low dynamics is relatively heavy and composed of soft material. We call it the *soft* object.

The second one, named *high rate* loop, handles the simulation and the haptic rendering with a small integration time-step, typically 1 ms, in order to correctly compute the dynamics of the deformations of a light and stiff object. This solid is called the *stiff* object.

The following notation is used throughout the remaining of the paper: for any mechanical variable, such as $\mathbf{M}$, the right subscript indicates the corresponding object, the left subscript represents in which simulation loop the value is computed ($L$ for the *low rate* loop, $H$ for the *high rate* one) and the left superscript represents which integration time-step is used to compute the variable. In our framework, two integration steps are used: $\Delta T$ which is the larger time-step and $dt$ which is the smaller time-step. For instance ${}^{dt}_{L}\mathbf{M}_{\text{stiff}}$ encodes the mass matrix of the object named *stiff*. This matrix is computed in the *low rate* simulation loop using an integration time-step of $dt$. The same notation is consistently derived to represent vectors: ${}^{dt}_{L}\mathbf{v}_{\text{soft}}$ is the velocity vector of the object *soft* being computed in the *low rate* loop using an integration time-step of $dt$.

### A. FEM-based deformable models

The deformable models used in our simulation are based on the finite element (FE) method. The materials are supposed to have linear elastic constitutive laws but geometric non-linearities occurs due to large deformations. Since the FE are in general quite computationally expensive, it is necessary to employ an efficient method to simulate the stiff object which is simulated at high frequency. In this work we employ serially linked beam elements that can fulfill the computation time requirements while handling properly the non-linear deformations [16]. On the contrary, the computation time for the *soft* object is less constrained. Therefore, a volume FE model composed of several hundreds of tetrahedral elements can be employed. To capture the geometrical nonlinearities, we rely on a corotational formulation [17].

In both cases, the FE models are composed of elements that integrate the material properties of the solids (mass, elasticity) and of nodes which are the degrees of freedom sampled over the deformable domains. Both deformable solids behave according to the equation of the dynamics:

$$\mathbf{M}\mathbf{a} = \mathbf{f}(\mathbf{x}, \mathbf{v}) + \mathbf{J}^T\lambda \tag{1}$$

where $\mathbf{a}$ denotes the acceleration of the nodes, $\mathbf{x}$ and $\mathbf{v}$ are respectively the node positions and velocities, $\mathbf{M}$ is the mass matrix and $\mathbf{f}$ is the sum of internal stiffness forces and external forces. Finally, the second term of the right-hand member of Eq. 1 stands for the constraints imposed on the solid: $\mathbf{J}^T$ provides the directions of constraints and $\lambda$ is the vector of constraint response forces.

The time integration is performed using a backward Euler integration scheme. Implicit integration is preferred to ensure stable behavior regardless the choice of the time-steps. Denoting $h$ the time-step used in the integration ($h = dt$ for the small time-step and $h = \Delta T$ for the large time-step), the backward Euler scheme provides the following equations:

$$\mathbf{v}^{t+h} = \mathbf{v}^t + h\mathbf{a}^{t+h} \qquad \mathbf{x}^{t+h} = \mathbf{x}^t + h\mathbf{v}^{t+h}. \tag{2}$$

The forces $\mathbf{f}$ are non-linear functions of positions $\mathbf{x}$ and velocities $\mathbf{v}$. We apply a Taylor series expansion to $\mathbf{f}$ and make the first order approximation (a single linearization by time-step):

$$\mathbf{f}(\mathbf{x}^{t+h}, \mathbf{v}^{t+h}) \approx \mathbf{f}(\mathbf{x}^t, \mathbf{v}^t) + \mathbf{K}(\mathbf{x}^{t+h} - \mathbf{x}^t) + \mathbf{B}(\mathbf{v}^{t+h} - \mathbf{v}^t) \tag{3}$$

where $\mathbf{f}$ represents the internal stiffness forces at a given position $\mathbf{x}$ of the degrees of freedom, $\mathbf{K}$ is the stiffness matrix depending on the current position. A damping matrix $\mathbf{B} = \alpha\mathbf{M} + \beta\mathbf{K}$ is introduced in the Eq. 3, where $\alpha$ and $\beta$ are respectively the *Rayleigh mass* and the *Rayleigh damping* coefficients. By combining equations (1) and (3) we get

$$\underbrace{(\frac{1}{h}\mathbf{M} - \mathbf{B} - h\mathbf{K})}_{\mathbf{A}}\,\mathbf{dv} \approx \underbrace{\mathbf{f}(\mathbf{x}^t, \mathbf{v}^t) + h\mathbf{K}\mathbf{v}^t}_{\mathbf{b}} + \mathbf{J}^t\lambda \tag{4}$$

where $\mathbf{dv}$ is defined as $\mathbf{dv} = h\mathbf{a} = \mathbf{v}^{t+h} - \mathbf{v}^t$. We emphasize that the matrix $\mathbf{A}$, which is recomputed in each step of the simulation, depends on the time-step $h$.

### B. Interaction Model

The FE models of both *stiff* and *soft* objects are linked by the constraint based expression of their mechanical interactions. Among the interactions between the two deformable bodies, we need to detect the collisions and provide an adequate response (without inter-penetration). The collision detection (or more generally the geometrical determination of the contact points) is often time consuming and is not compatible with the *high rate* loop. In our approach, we use an algorithm based on *proximity queries* between FE meshes that is computed in the *low rate* loop. It is supposed that we have access to the geometrical position of the *stiff* object in the *low rate* loop. The algorithm places contact constraints where the local minimal distance between the meshes is small enough to have a potential collision between current time $t$ and $t + \Delta T$. Other type of constraints, for instance bilateral constraints (attachment, sliding..) can also be set. After computing the queries, a matrix $\mathbf{J}$ containing the directions of unilateral and bilateral constraints for each object is assembled.

To handle the contacts realistically, we rely on the Signorini's law[1] $0 \leq \boldsymbol{\delta} \perp \boldsymbol{\lambda} \geq 0$ where $\boldsymbol{\delta}$ represents the signed distances between potential contact points detected by the proximity queries. The bilateral constraints prevent the relative motion of the bodies at given point and direction. Thus, at this point the relative distance is forced to $\boldsymbol{\delta} = 0$. The constraints are set in the *low rate* loop but a very important feature of our method is that the resolution of the constraints is performed at both *high* and *low* rates, in order to have adequate constraint response on both dynamic models.

To solve the reaction forces of this response, we first need to evaluate the constraint violation when applying an unconstrained dynamic motion to both deformable objects

[1]We can also set additional constraints to simulate the friction with Coulomb's law like it is done in [6].

(i. e. solving Eq.(4) with $\boldsymbol{\lambda} = 0$.). This unconstrained motion is also called *free* motion and denoted by super-script in the equations. Computed on the *stiff* and *soft* objects with respectively small $h = dt$ and large $h = \Delta T$ time-steps, they provide the positions ${}^{dt}_{H}\mathbf{x}^{\text{free}}_{\text{stiff}}$ and ${}^{\Delta T}_{L}\mathbf{x}^{\text{free}}_{\text{soft}}$. However, to obtain a measure of the violation for both $h = dt$ and $h = \Delta T$, we also need to compute a value for ${}^{dt}_{L}\mathbf{x}^{\text{free}}_{\text{soft}}$ and ${}^{\Delta T}_{L}\mathbf{x}^{\text{free}}_{\text{stiff}}$ (i.e. the free position for the *soft* object with $h = dt$ and for the *stiff* object with $h = \Delta T$).

To obtain these position values it is required to solve two additional linear systems of equations. This is not an issue for the *stiff* solid because the cost of solving its system at *low rates* can be neglected. On the contrary, for the *soft* object, the corresponding system can be quite large and therefore, the value ${}^{dt}_{L}\mathbf{x}^{\text{free}}_{\text{soft}}$ is computed at *low rates*. This approximation is valid because the *soft* body has a *low* dynamic response. If it were computed at *high rate*, the displacement created by the unconstrained motion ${}^{dt}_{H}\mathbf{x}^{\text{free}}_{\text{soft}} - {}^{dt}_{H}\mathbf{x}_{\text{soft}}$ would not change much between *high rate* steps.

When obtaining the violation $\boldsymbol{\delta}^{\text{free}}$ at both *low* and *high* rates, we need to solve at both *low* and *high* rates a *mixed complementarity problem* (MCP). First we compute the MCP at *low rates*, with a time-step $\Delta T$:

$$\begin{cases} \boldsymbol{\delta} = \underbrace{\left[{}^{\Delta T}_{L}\mathbf{W}_{\text{soft}} + {}^{\Delta T}_{L}\mathbf{W}_{\text{stiff}}\right]}_{{}^{\Delta T}_{L}\mathbf{W}} \boldsymbol{\lambda} + {}^{\Delta T}_{L}\boldsymbol{\delta}^{\text{free}} \\ 0 \leq \boldsymbol{\delta} \perp \boldsymbol{\lambda} \geq 0 \text{ (for contact constraints)} \\ \boldsymbol{\delta} = 0 \qquad\quad \text{(for bilateral constraints)} \end{cases} \tag{5}$$

where the compliance matrices for soft and stiff objects are computed as

$$\begin{aligned} {}^{\Delta T}_{L}\mathbf{W}_{\text{soft}} &= {}_{L}\mathbf{J}_{\text{soft}}\ {}^{\Delta T}_{L}\mathbf{A}^{-1}_{\text{soft}}\ {}_{L}\mathbf{J}^{T}_{\text{soft}} \\ {}^{\Delta T}_{L}\mathbf{W}_{\text{stiff}} &= {}_{L}\mathbf{J}_{\text{stiff}}\ {}^{\Delta T}_{L}\mathbf{A}^{-1}_{\text{stiff}}\ {}_{L}\mathbf{J}^{T}_{\text{stiff}} \end{aligned} \tag{6}$$

As in the case of the *free* motion, we need to compute the compliance matrix of the *stiff* object with large time-steps $h = \Delta T$ in order to have an adequate response of the constraints at *low* rate. This is important as for dynamic systems, the value of the matrix $\mathbf{A}$ defined at Eq.(4) depends on the time-step $h$ as stated previously.

For the MCP at *high rates*, we use constraint violation ${}^{dt}_{H}\boldsymbol{\delta}^{\text{free}}$ computed using the position obtained at *high rates*. Additionally, we compute the compliance matrices obtained with small time-step $h = dt$. For the *stiff* object, the matrix ${}^{dt}_{H}\mathbf{A}_{\text{stiff}}$ is recomputed at *high rates*, and as the object has a fast dynamic response, important changes in ${}^{dt}_{H}\mathbf{A}_{\text{stiff}}$ can be observed between two small time-steps $dt$. However, we assume that the directions of constraints in $\mathbf{J}_{\text{stiff}}$ can be provided by the *low rate* loop in order to avoid an update of the proximity queries algorithm. This is valid only if these directions do not change significantly in the *high rate* loop between two updates. Thus, the computation of the compliance matrix of the *stiff* object is:

$${}^{dt}_{H}\mathbf{W}_{\text{stiff}} = {}_{L}\mathbf{J}_{\text{stiff}}\,{}^{dt}_{H}\mathbf{A}^{-1}_{\text{stiff}}\ {}_{L}\mathbf{J}^{T}_{\text{stiff}} \tag{7}$$

It must be emphasized that the computational cost needed for this matrix must be compatible with the real-time requirement imposed on the *high rate* loop.

Finally, we need to compute the compliance ${}^{dt}\mathbf{W}_{\text{soft}}$ of the *soft* object employing the small time-step $h = dt$; this quantity can be regarded as an *apparent compliance*, i. e. the compliance of the *soft* object observed in the high-rate simulation loop. The computation of this matrix is expensive as it involves the inverse of the matrix $\mathbf{A}_{\text{soft}}$ which is not optimal for an update at *high rates*. However, as the *soft* object has a low dynamic response, we estimate that ${}^{dt}\mathbf{A}_{\text{soft}}$ does not change much between two time-steps computed at *low rates*. Thus, the computation of the compliance matrix ${}^{dt}\mathbf{W}_{\text{soft}}$ is performed at *low rates*:

$${}^{dt}_{L}\mathbf{W}_{\text{soft}} = {}_{L}\mathbf{J}_{\text{soft}}\,{}^{dt}_{L}\mathbf{A}^{-1}_{\text{soft}}\ {}_{L}\mathbf{J}^{T}_{\text{soft}}. \tag{8}$$

Finally, the values computed at *low rates* are shared with the *high rates* loop, so that the MCP can be resolved at *high rates*:

$$\begin{cases} \boldsymbol{\delta} = \underbrace{\left[{}^{dt}_{L}\mathbf{W}_{\text{soft}} + {}^{dt}_{H}\mathbf{W}_{\text{stiff}}\right]}_{{}^{dt}_{L}\mathbf{W}} \boldsymbol{\lambda} + {}^{dt}_{H}\boldsymbol{\delta}^{\text{free}} \\ 0 \leq \boldsymbol{\delta} \perp \boldsymbol{\lambda} \geq 0 \text{ (for contact constraints)} \\ \boldsymbol{\delta} = 0 \qquad\quad \text{(for bilateral constraints)} \end{cases} \tag{9}$$

The resolution of this MCP provides an adequate response for the constraints on the *stiff* object simulated at *high rates*.

Overall, to build the 2 MCPs, three compliance matrices are computed at *low rates* (two matrices with two different time-steps $dt$ and $\Delta T$ for the *soft* object and one matrix with time-step $\Delta T$ for the *stiff* object). One compliance matrix is computed at *high rates* for the *stiff* object with the small time-step $dt$. Consequently it can be observed that the method provides additional computations at *low rates* for obtaining adequate compliance matrices, but these computations can be easily parallelized.

After the MCP is solved, a corrective motion is applied to each object. This step consists of solving Eq. 4 with the new value of $\boldsymbol{\lambda}$ and setting $\mathbf{b} = 0$. Then, as the system in Eq. 4 is linear, we can compute the final motion by adding the displacements obtained by corrective motion to those calculated by free motion at the beginning of the time step.

## IV. Computational Model

In this part, the computational model showing the implementation of two threads and structures shared between them is given in detail. The symbols introduced in the previous section are employed to denote the vectors and matrices corresponding to the objects simulated at different frequencies.

### A. Multi-rate algorithm for dynamic modeling

The simulation is performed in two separated threads each running at different frequency. The first thread implements the *high rate* loop of the simulation in which the dynamics of the *stiff* object is computed and directly coupled to the haptic force feedback. In the second thread, the dynamics of the *soft* object is modeled, together with full resolution of the

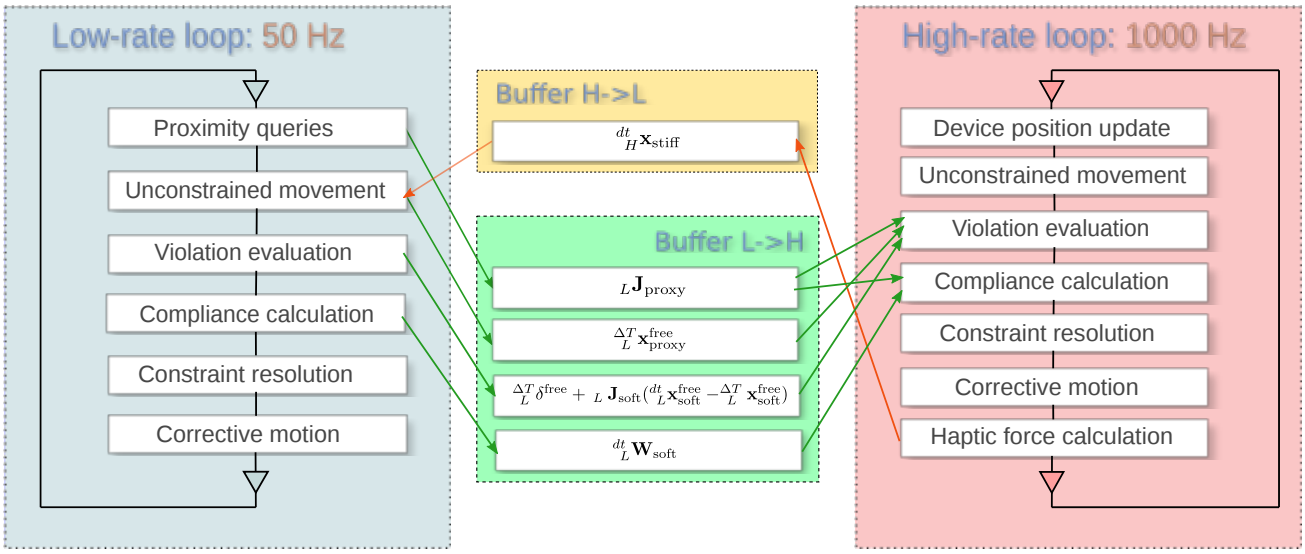


Fig. 1. Schematic visualization of the computational model.

MCP being in charge of constraint resolution as described in section III-B.

In each time-step of the *low rate* loop, seven sub-steps L1 — L7 are performed as follows:

L1 Potential collisions are detected using *proximity queries* which are evaluated using the position vectors ${}_{L}\mathbf{x}_{\text{proxy}}$ and ${}_{L}\mathbf{x}_{\text{soft}}$ computed in the last sub-step of the previous time-step. The calculation results in matrices ${}_{L}\mathbf{J}_{\text{proxy}}$ and ${}_{L}\mathbf{J}_{\text{soft}}$. Both matrices are stored to the buffer to be available to the *high rate* loop.

L2 The position of the *stiff* object ${}_{H}\mathbf{x}_{\text{stiff}}$ computed in the sub-step H6 of the previous *high rate* loop time-step is imposed to the *proxy*.

L3 The unconstrained dynamics of each object is simulated: first, using $\Delta T$ for both *proxy* and *soft*, the system matrices (4) are assembled and inverted resulting in $^{\Delta T}_{L}\mathbf{A}^{-1}_{\text{proxy}}$ and $^{\Delta T}_{L}\mathbf{A}^{-1}_{\text{soft}}$ and unconstrained positions are computed and stored in vectors $^{\Delta T}_{L}\mathbf{x}^{\text{free}}_{\text{proxy}}$, $^{\Delta T}_{L}\mathbf{x}^{\text{free}}_{\text{soft}}$. Second, the calculation is repeated for the *soft* object, however, *high rate* time-step $dt$ is used instead of $\Delta T$ to compute the system matrix, resulting in inverted matrix $^{dt}_{L}\mathbf{A}^{-1}_{\text{soft}}$ and unconstrained position vector $^{dt}_{L}\mathbf{x}^{\text{free}}_{\text{soft}}$.

L4 The constraint violation $^{\Delta T}_{L}\boldsymbol{\delta}^{\text{free}}$ is computed as shown in section III-B. An additional correction term is computed as ${}_{L}\mathbf{J}_{\text{soft}}\left(^{dt}_{L}\mathbf{x}^{\text{free}}_{\text{soft}} - ^{\Delta T}_{L}\mathbf{x}^{\text{free}}_{\text{soft}}\right)$. This term is necessary for the calculation of constraint violation in the *high rate* loop as shown in H3. Both the violation and corrective term vectors are stored in the buffer.

L5 Two compliance matrices, $^{\Delta T}_{L}\mathbf{W}_{\text{proxy}}$ and $^{\Delta T}_{L}\mathbf{W}_{\text{soft}}$ are computed for each object using $^{\Delta T}_{L}\mathbf{A}^{-1}_{\text{proxy}}$ and $^{\Delta T}_{L}\mathbf{A}^{-1}_{\text{soft}}$. One compliance matrix $^{dt}_{L}\mathbf{W}_{\text{soft}}$ is computed for the *soft* object using $^{dt}_{L}\mathbf{A}^{-1}_{\text{soft}}$. The latter is stored to the buffer.

L6 The constraint resolution is performed in the *low rate* loop using the compliance $^{\Delta T}_{L}\mathbf{W} = ^{\Delta T}_{L}\mathbf{W}_{\text{soft}} + ^{\Delta T}_{L}\mathbf{W}_{\text{stiff}}$ and the vector $^{\Delta T}_{L}\boldsymbol{\delta}^{\text{free}}$ computed in L4, resulting in the vector of corrective forces $^{\Delta T}_{L}\boldsymbol{\lambda}$.

L7 Finally, the force vector $^{\Delta T}_{L}\boldsymbol{\lambda}$ is used to apply the motion correction to both *proxy* and the *soft* objects resulting in constrained positions $^{\Delta T}_{L}\mathbf{x}_{\text{proxy}}$ and $^{\Delta T}_{L}\mathbf{x}_{\text{soft}}$.

The *high rate* simulation loop running in parallel performs 6 sub-steps in one time-step employing the data buffered in the last time-step of the *low rate* loop as follows:

H1 The position representing the location of the haptic interaction point is updated according to the actual position of the haptic device.

H2 The unconstrained position $^{dt}_{H}\mathbf{x}^{\text{free}}_{\text{stiff}}$ of the *stiff* object is computed using the inverse $^{dt}_{H}\mathbf{A}^{-1}_{\text{stiff}}$ of the system matrix.

H3 The constraint violation $^{dt}_{H}\boldsymbol{\delta}^{\text{free}}$ is computed. It is not possible to use directly the violation $^{\Delta T}_{L}\boldsymbol{\delta}^{\text{free}}$ calculated in L4 of the *low rate* loop, since this vector was computed from unconstrained position simulated with a different time-step $\Delta T$. Nevertheless, the desired *high rate* violation can be obtained as follows:

$$^{dt}_{H}\boldsymbol{\delta}^{\text{free}} = ^{\Delta T}_{L}\boldsymbol{\delta}^{\text{free}} \tag{10}$$

$$+ \ {}_{L}\mathbf{J}_{\text{soft}}\left(^{dt}_{L}\mathbf{x}^{\text{free}}_{\text{soft}} - ^{\Delta T}_{L}\mathbf{x}^{\text{free}}_{\text{soft}}\right) \tag{11}$$

$$+ \ {}_{L}\mathbf{J}_{\text{proxy}}\left(^{dt}_{H}\mathbf{x}^{\text{free}}_{\text{stiff}} - ^{\Delta T}_{L}\mathbf{x}^{\text{free}}_{\text{proxy}}\right) \tag{12}$$

where (11) is a corrective term compensating for the different time-step in *soft* object dynamics computed in L4 and (12) is a similar corrective term computed here using the unconstrained positions of the *proxy* and *stiff* objects calculated in L3 and H2, respectively.

H4 The compliance matrix $^{dt}_{H}\mathbf{W}$ is computed as a sum of $^{dt}_{L}\mathbf{W}_{\text{soft}}$ computed in L5 and

$$^{dt}_{H}\mathbf{W}_{\text{stiff}} = \left\{ {}_{L}\mathbf{J}_{\text{proxy}} \right\} \left\{ ^{dt}_{H}\mathbf{A}^{-1}_{\text{stiff}} \right\} \left\{ {}_{L}\mathbf{J}^{\top}_{\text{proxy}} \right\}.$$

H5 The time-limited constraint resolution is performed using $^{dt}_{H}\mathbf{W}$ from H4 and $^{dt}_{H}\boldsymbol{\delta}^{\text{free}}$ from H3, resulting in

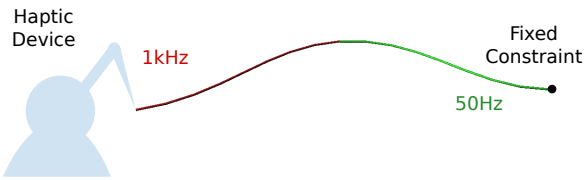


Fig. 2. Illustration of the two beams example. Deformations are the same at *low rates* (green) and at *high rates* (red).

correction force vector ${}^{dt}_{H}\boldsymbol{\lambda}$.

H6 The forces stored in ${}^{dt}_{H}\boldsymbol{\lambda}$ are used to compute the corrected position ${}^{dt}_{H}\mathbf{x}_{\text{stiff}}$ of the *stiff* object. The position ${}^{dt}_{H}\mathbf{x}_{\text{stiff}}$ is stored to the buffer to be available for the *low rate proxy* object needed in sub-step L2.

### B. Force-feedback for haptic rendering

As described in the previous section, the dynamics of the *stiff* body is computed in the *high rate* loop as realistic simulation of its behavior requires small time-step. Moreover, this body usually represents the object (such as the deformable needle) which is driven by the user. However, this means that this tool is attached to the haptic device and the force response of the tool represents the force-feedback which should be delivered to the user via the haptic device.

In our setting, the vector ${}^{dt}_{H}\boldsymbol{\lambda}$ computed in H5 gathers the actual forces corresponding to the constraints imposed on both *soft* and *stiff* objects. In order to compute the response force in the nodes of the stiff object corresponding to the constraint forces, the constraint forces has to be transformed from the constraint space to the space of degrees of freedom of the *stiff* object. This is done using the matrix ${}_{L}\mathbf{J}_{\text{proxy}}$ which contains the constraint directions computed in sub-step L1 as $\mathbf{f}_{\text{stiff}} = \{ {}_{L}\mathbf{J}_{\text{proxy}} \}^{dt}_{H} \boldsymbol{\lambda}$ where $\mathbf{f}_{\text{stiff}}$ is the vector of forces applied in the nodes of the *stiff* object due to the constraints imposed on the *stiff* object. Finally, the force feedback is calculated by summing the vector $\mathbf{f}_{\text{stiff}}$ over the nodes of the stiff object, i. e. $\mathbf{f}_{\text{haptic}} = \sum_n \mathbf{f}^n_{\text{stiff}}$.

## V. Results

In this section we present results of experiments demonstrating the multi-rate method presented in this paper. A companion video is available illustrating the following results.

The first experiments highlight the action-reaction principle. We propose a basic scenario which allows to verify that the principle is preserved in simulation implemented according to our method. Two beam models composed of 10 segments each with identical mechanical parameters (Young's modulus of 10 GPa, mass of 0.01 kg and with a length of 20 cm) are connected with a bilateral constraint. The other end of the *low rate* beam model is fixed in the space, whereas the free end of the *high rate* beam model is attached to the haptic device. The experiment shows that although being computed at different frequencies, the beams undergo symmetric deformations for arbitrary position of the haptic device after the simulation is stabilized. Moreover, the dynamics of the *high rate* beam accounts for *high rate* vibrations observed during the simulation.

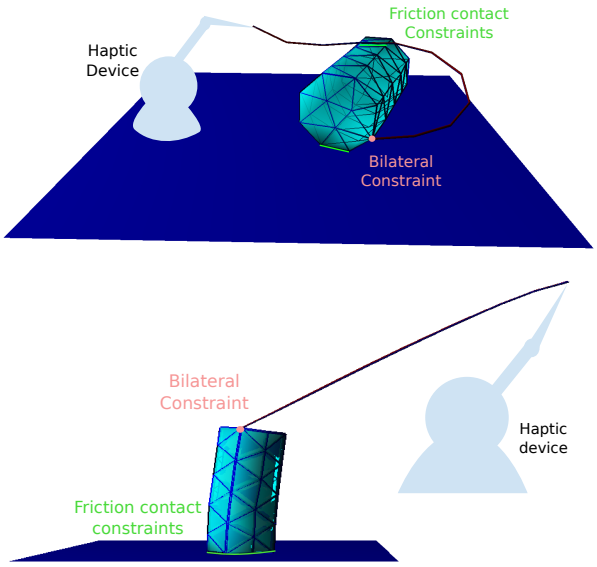


Fig. 3. Illustration of the scene composed by a cylinder (simulated at 50 Hz) and a thread (simulated at 1 kHz).

To validate our approach, we created another simulation scene where a cylinder is placed on a horizontal plane. The cylinder is modeled by tetrahedral corotational FEM with 100 tetrahedra and is simulated at 50 Hz. A wire is attached to the upper part of the cyliner and the other endpoint of the thread is driven by a haptic device as shown in Fig. 3. The wire is modeled with 10 serially-linked beam elements based on Tymoshenko formulation and its dynamics is computed at 1000 Hz. The dimensions of the cylinder are 8 cm (height) and 2 cm (radius) and its Young's modulus is set to 15 kPa, mass being 0.1 kg. The wire is 20 cm long, having a mass of 0.01 kg and Young's modulus of 10 GPa. The collisions between the plane, cylinder and the thread are being detected and resolved during the simulation. During the interaction, the simulation remains stable for any admissible configuration: the position of the cylinder on the plane can be changed by pulling the wire, or the cylinder can be even pulled out of the plane, so it's hanging freely in the space, being attached with the wire. At the same time, a detailed and realistic haptic force-feedback is delivered to the user via the mechanism described in section IV-B.

## VI. Conclusion and Future Work

The main contribution of the paper is in presenting a novel method allowing the simulation of dynamic deformable models computed at different frequencies. The collisions between the objects are handled correctly according to the Signorini's law and the force feedback delivered to the user through a haptic interface is based on accurate physics-based principles. While additional computational overhead is introduced in the *low rate* loop, where three compliance matrices are computed, the calculations in the *high rate*

thread remain compatible with the frequency of 1000 Hz required by the haptic rendering.

Examples has been provided to demonstrate that the action-reaction principle is well preserved in the simulation and further, the *high rate* response allows for correct rendering of such phenomena as high-frequency vibration of the thread, which rapidly increases quality of haptic rendering of light and stiff objects such as wires and needles.

There are some limitations to the method that will be addressed in the future work. First, no theoretical proof of the haptic feedback stability has been presented so far. While the tests presented in this paper exhibit realistic and stable behavior when force feedback is activated, a more formal proof of the stability should be provided. Second, the actual implementation and the examples presented in the paper show only two objects in collision running at two different frequencies. While we believe such scenario already opens a wide range of possibilities for many applications in virtual reality, extending our approach to scenarios with more than two frequencies should be investigated. Simulations that include several deformable models being computed at their optimal frequencies would enable more complex simulations without sacrificing the realism, accuracy and quality of dynamic response. However, scaling our approach to many simulation frequencies may drastically increase the computational burden as well as the volume of data shared among the simulation loops. Therefore future work will aim at proposing a generic way to handle multi-rate simulations while reducing the computational overhead to handle the interactions.

## REFERENCES


[1] J. Dequidt, L. Grisoni, and C. Chaillou, "Collaborative interactive physical simulation," in *GRAPHITE '05: Proceedings of the 3rd international conference on Computer graphics and interactive techniques in Australasia and South East Asia*, S. Spencer, Ed. ALCOVE (INRIA / LIFL), Dec. 2005, pp. 147–150. [Online]. Available: http://is.gd/DqSgXg

[2] I. Peterlik, C. Duriez, and S. Cotin, "Asynchronous haptic simulation of contacting deformable objects with variable stiffness," in *Intelligent Robots and Systems (IROS), 2011 IEEE/RSJ International Conference on*, Sept., pp. 2608–2613.

[3] M. Bro-Nielsen and S. Cotin, "Real-time volumetric deformable models for surgery simulation using finite elements and condensation," *Computer Graphics Forum*, vol. 15, no. 3, pp. 57–66, 1996.

[4] D. C. Popescu and M. Compton, "A model for efficient and accurate interaction with elastic objects in haptic virtual environments," in *GRAPHITE '03: Proceedings of the 1st international conference on Computer graphics and interactive techniques in Australasia and South East Asia*, 2003, pp. 245–250.

[5] D. L. James and D. K. Pai, "A unified treatment of elastostatic contact simulation for real time haptics," in *SIGGRAPH '05: ACM SIGGRAPH 2005 Courses*, 2005, p. 141.

[6] C. Duriez, F. Dubois, A. Kheddar, and C. Andriot, "Realistic haptic rendering of interacting deformable objects in virtual environments," *IEEE Transactions on Visualization and Computer Graphics*, vol. 12, no. 1, pp. 36–47, 2006.

[7] J. Barbič and D. L. James, "Six-dof haptic rendering of contact between geometrically complex reduced deformable models," *IEEE Trans. Haptics*, vol. 1, no. 1, pp. 39–52, 2008.

[8] G. Saupin, C. Duriez, and S. Cotin, "Contact model for haptic medical simulations," in *ISBMS '08: Proceedings of the 4th international symposium on Biomedical Simulation*. Berlin, Heidelberg: Springer-Verlag, 2008, pp. 157–165.

[9] C. Garre and M. A. Otaduy, "Haptic rendering of complex deformations through handle-space force linearization," *World Haptics Conference*, vol. 0, pp. 422–427, 2009.

[10] P. Jacobs, M. J. Fu, and M. C. Cavusoglu, "High Fidelity Haptic Rendering of Frictional Contact with Deformable Objects in Virtual Environments using Multi-rate Simulation," *The International Journal of Robotics Research*, Sept. 2010. [Online]. Available: http://ijr.sagepub.com/cgi/doi/10.1177/0278364910378540

[11] D. Harmon, E. Vouga, B. Smith, R. Tamstorf, and E. Grinspun, "Asynchronous contact mechanics," *ACM Transactions on Graphics*, vol. 28, no. 3, p. 1, July 2009. [Online]. Available: http://portal.acm.org/citation.cfm?doid=1531326.1531393

[12] S. Ainsley, E. Vouga, E. Grinspun, and R. Tamstorf, "Speculative parallel asynchronous contact mechanics," *ACM Trans. Graph.*, vol. 31, no. 6, pp. 151:1–151:8, Nov. 2012. [Online]. Available: http://doi.acm.org/10.1145/2366145.2366170

[13] D. Harmon, Q. Zhou, and D. Zorin, "Asynchronous integration with phantom meshes," in *Proceedings of the 2011 ACM SIGGRAPH/Eurographics Symposium on Computer Animation*, ser. SCA '11. New York, NY, USA: ACM, 2011, pp. 247–256. [Online]. Available: http://doi.acm.org/10.1145/2019406.2019439

[14] I. Susa, M. Sato, and S. Hasegawa, "Multi-rate multi-range dynamic simulation for haptic interaction," in *World Haptics Conference (WHC), 2011 IEEE*, June, pp. 233–238.

[15] G. Böttcher, D. Allerkamp, and F.-E. Wolter, "Multi-rate coupling of physical simulations for haptic interaction with deformable objects," *The Visual Computer*, vol. 26, no. 6-8, pp. 903–914, Apr. 2010. [Online]. Available: http://www.springerlink.com/index/10.1007/s00371-010-0450-1

[16] C. Duriez, S. Cotin, J. Lenoir, and P. F. Neumann, "New approaches to catheter navigation for interventional radiology simulation," *Computer Aided Surgery*, vol. 11, no. 6, pp. 300–308, 2006.

[17] C. Felippa and B. Haugen, "A unified formulation of small-strain corotational finite elements: I. theory," *Computer Methods in Applied Mechanics and Engineering*, vol. 194, no. 21, pp. 2285–2335, 2005.